



Contents lists available at ScienceDirect

Journal of Loss Prevention in the Process Industries

journal homepage: www.elsevier.com/locate/jlp

Methane-induced explosions in vented enclosures

Hayri Sezer^{a, b, *}, Francis Kronz^a, V'yacheslav Akkerman^a, Ali S. Rangwala^b^a Department of Mechanical and Aerospace Engineering, Center for Innovation in Gas Research and Utilization (CIGRU), West Virginia University, Morgantown, WV 26506-6106, USA^b Department of Fire Protection Engineering, Worcester Polytechnic Institute, Worcester, MA 01609, USA

ARTICLE INFO

Article history:

Received 18 October 2016

Received in revised form

10 April 2017

Accepted 11 April 2017

Available online 14 April 2017

Keywords:

Vented explosions

Enclosures

External explosion

Methane

Overpressures

NFPA 68

ABSTRACT

Explosions in enclosures leading to devastating accidents occur in various industrial, commercial, and residential occupancies. To relieve the effect of such explosions, vents of various sizes and geometry are designed. In this study, a computational model for gas explosions venting, developed and validated on hydrogen explosion by Ugarte et al. [*Process Safety and Environmental Protection*, 99, (2016) 167–174] is extended to vented explosion scenarios for methane. The model is based on a time-dependent set of ordinary differential equations whose solution allows prediction of temperature, pressure and vented mass transients resulting from the explosion of methane-air in vented enclosures. The model is compared to the experiments available in the literature and NFPA 68 standards at different vent areas and equivalent ratios. The influence of gas equivalence ratio and vent size on the rate of pressure rise is analyzed. A framework for the gas explosion vent design using the fundamental laminar burning velocity of a gas-air mixture is also discussed.

© 2017 Elsevier Ltd. All rights reserved.

1. Introduction

Circumventing explosions resulting from premixed combustion in enclosures is a vital issue for industry and home safety because the devastation from the gas explosions may end up with catastrophic consequences. Therefore, it is important to investigate the effect of fuel composition and enclosure configuration on explosions in enclosures (Faghih et al., 2016; Ugarte et al., 2016). To relieve the effect of explosions, vents of various sizes and configurations are incorporated into enclosures (STANDARD, 2008; Tamanini and Valiulis, 1996). Mathematical models can reveal important features of vented enclosures that can be employed during a research-and-development (R&D) stage of explosion safety standards. These models can be classified as follows: **1**) analytical equations and correlations for vent area (Forcier and Zalosh, 2000); **2**) simplified reduced-order models (Molkov et al., 2000; Sezer et al., 2016), and **3**) detailed computational fluid dynamics (CFD) models (Zalosh, 2008; Bauwens et al., 2011). In this respect, analytical equations and correlations, based on the

experimental data, can be limited in terms of the accurate quantitative prediction of the evolution of the combustion process. The detailed CFD models are usually expensive from the viewpoint of computational time and cost. In addition, oftentimes, they are complicated and hard to employ and revisit. The reduced-order phenomenological computational models can be used to reveal the explosion behavior for complex situations (Zalosh, 2008). Specifically, the governing equations for the gas explosions in a three-dimensional (3-D) space are reduced to 0-D (only time-dependent) set of ordinary differential equations (ODEs) as dealt in the present work, where an in-house phenomenological computational model for gas explosion venting, named the Explosive Vent Analyzer (EVA), is implemented. EVA was developed and validated on hydrogen explosions by Ugarte et al. (2016), and it is herein extended to predict the pressure and vented mass transients resulting from the explosion of methane-air in vented enclosures. The interested readers are referred to Refs (Ugarte et al., 2016; Mulpuru and Wilkin, 1982) for the details of EVA. For the methane explosions scenarios, the computational model is modified to calculate the thermodynamic properties of methane-air mixtures by means of coupling the NASA-CAE (Sanford and McBride, 1996) computer code with the model (Ugarte et al., 2016). Moreover, the NASA tool incorporated in the model can

* Corresponding author. Department of Fire Protection Engineering, Worcester Polytechnic Institute, Worcester, MA 01609, USA.

E-mail addresses: hsezer@mix.wvu.edu, hsezer@wpi.edu (H. Sezer).

calculate the thermochemical properties of several fuel-air mixtures listed in the NASA database. The laminar methane-air burning velocities are taken from (Stone et al., 1998). In the present work, a detailed parametric study of vented enclosures is performed for various equivalent ratios and venting areas. The results are compared to NFPA 68 standards for gas explosions and the experimental data by Bao et al. (2016) and Bauwens et al. (2008).

2. Model description

The explosion venting analyzer (EVA) is a 0-D, transient phenomenological model developed to predict the evolution of the overpressure, vented mass, and the flame speed during the explosion process. The EVA can be used to predict the peak overpressure and pressure rise for the spherical, cylindrical, and cuboid enclosure geometries with a single vent. EVA's chronological development [2, 6, 8] and limitations are listed in Table 1. The flame shape in a cuboid is estimated based on the experimental work by Cooper et al. (1986), namely, it is modeled as a half-sphere, half-ellipsoid in the case of central ignition; and as a half-ellipsoid for rear ignition. EVA can be employed to calculate the minimum vent area required by explosion venting design codes, for example, (NFPA 68, 2013), where the minimum vent area, A_{v0} is given by:

$$A_{v0} = \begin{cases} \frac{A_s C}{\sqrt{P_{red}}}, & P_{red} > 0.5 \text{ bar} \\ A_s \left[\frac{1 - \left(\frac{P_{red} + 1}{P_{max} + 1}\right)^{1/\gamma_b}}{\left[\left(\frac{P_{red} + 1}{P_{max} + 1}\right)^{1/\gamma_b} - \delta\right]} \right] \frac{S_u \rho_u \lambda}{G_u C_d}, & P_{red} > 0.5 \text{ bar} \end{cases} \quad (1-a)$$

with,

$$C = \frac{S_u \rho_u \lambda}{2G_u C_d} \left[\left(\frac{P_{max} + 1}{P_0 + 1}\right)^{1/\gamma_b} - 1 \right] (P_0 + 1)^{1/2} \text{ and } \delta = \frac{\left(\frac{P_{stat} + 1}{P_0 + 1}\right)^{1/\gamma_b} - 1}{\left(\frac{P_{max} + 1}{P_0 + 1}\right)^{1/\gamma_b} - 1}. \quad (1-b)$$

A_s is the enclosure surface area, P_{max} is the maximum pressure developed in a confined deflagration, P_0 , is the initial pressure, P_{red} is the maximum pressure developed in a vented enclosure during a vented deflagration, P_{stat} is nominal vent deployment or burst pressure and S_u , ρ_u , and G_u are the fundamental burning velocity, density, and sonic flow mass flux of unburnt gas-air mixture respectively. C_d , γ_b and λ are constants equal to the vent flow discharge coefficient, ratio of the specific heats of the burned gas, and the ratio of gas-air mixture turbulent burning velocity to the laminar burning velocity respectively. P_{max} as well as the thermo-physical properties of the gaseous mixture, γ_b , ρ_u and S_u can be calculate by the EVA. Furthermore, the turbulent to laminar burning velocities ratio λ can be calculated by a three different formulations that is available in the EVA (See (Ugarte et al., 2016)). Therefore, EVA can potentially be used to determine the minimum vent area. In the present study, the EVA is validated by the experimental results of Bao et al. (2016), and also compared to a detailed CFD study by Bauwens et al. (2008) that includes the spatial variations of pressure, burning velocity, and vented mass transients. The validated model is then used to perform a parametric study of explosion pressure on vent size for methane-air mixtures in a

cubical compartment.

3. Mathematical formulation

The EVA solver uses a reduced-order mathematical model for explosion characteristics in vented enclosures (Fig. 1) first derived by Mulpuru and Wilkin (1982). The model equations were extended to include the flame shape, burning velocity, enclosure shape, and external explosion by Ugarte et al. (2016). The model assumptions are:

- (1) Point source ignition
- (2) Ideal gas
- (3) Isentropic compression and expansion of the unburned gas
- (4) Uniform gas properties and pressure distribution
- (5) Negligible acoustic effects (Harrison and Eyre, 1987)
- (6) Negligible obstructions for flame propagation

The mass balance inside the enclosure can be written as (Mulpuru and Wilkin, 1982)

$$\frac{d}{dt} \left(\frac{m_u}{m_i} \right) + \frac{d}{dt} \left(\frac{m_b}{m_i} \right) + \frac{d}{dt} \left(\frac{m_v}{m_i} \right) = 0, \quad (2)$$

where the subscripts u , b , v and i designate the unburned, burned, vented and initial conditions, respectively, while m and t stand for mass and time. Equation (2) is subsequently modified assuming that the process is isentropic ($P/\rho^{\gamma_u} \equiv \text{Constant}$) to obtain an expression in terms of the instantaneous pressure, \bar{P} , the fraction of the initial volume occupied by the burnt gas, \bar{V} , and initial mass fraction of the burnt gas, n ; see Refs. (Ugarte et al., 2016; Mulpuru and Wilkin, 1982) for more details of the transformation. The energy balance equation in the vented enclosure is given by (Mulpuru and Wilkin, 1982)

$$\frac{d}{dt} \left(\frac{m_u E_u}{m_i} \right) + \frac{d}{dt} \left(\frac{m_b E_b}{m_i} \right) + E_u \frac{d}{dt} \left(\frac{m_v}{m_i} \right) = 0, \quad (3)$$

where $E = e_0 + e(T) + e(T_0)$ comprises the energy of formation, e_0 and the change of the internal energy from the reference temperature (i.e. $T_0 = 298K$). Assuming that the process is isentropic, and the relations obey the ideal gas approximation, Eq. (3) can be expressed in terms of \bar{P} , \bar{V} and n . Equations (2)–(3) expressed in terms of the scaled variables \bar{P} , \bar{V} and n constitute a system of ODEs, which is solved by means of the fourth-order Runge-Kutta method to ensure the accuracy of the numerical solution; see Refs (Ugarte et al., 2016; Mulpuru and Wilkin, 1982) for more details. Another important characteristic of the combustion process is the unsteady burning velocity which is related to the reaction rates of the chemical reactions that are involved in the combustion process, being functions of the equivalence ratio, pressure, and temperature of the reactants (Stone et al., 1998; Sharma et al., 1981; Liao et al., 2004). Specifically, the unsteady burning velocity is given by (Stone et al., 1998; Liao et al., 2004)

$$S_L = S_{L,0} \left(\frac{T_u}{T_{u,0}} \right)^\alpha \left(\frac{P_u}{P_{u,0}} \right)^\beta, \quad (4)$$

where $S_{L,0}$ is the laminar burning velocity at the initial temperature and pressure, and the exponents α and β are usually functions of the fuel/air equivalence ratio ϕ . In this study, we employ the parameters $S_{L,0}$, α and β from (Stone et al., 1998), namely

$$S_{L,0} = 37.6 + 15.1(\phi - 1) - 221(\phi - 1)^2 - 45.8(\phi - 1)^3 + 358(\phi - 1)^4, \quad (5)$$

$$\alpha = 1.42 + 1.98(\phi - 1); \quad \beta = -0.314 + 608(\phi - 1)$$

Together, Eqs. (4) and (5) identify the methane-air unsteady burning velocity.

4. Validation

In order to validate the EVA, two sets of methane-air gas deflagration experiments in enclosures with single vents from the literature were used: first, various venting pressures were studied in the experiments by Bao et al. (2016); second, the experiments and CFD simulations for vented enclosures by Bauwens et al. (2008) were considered. Both studies use natural gas (~95% methane) the most common cause of explosions in buildings, and the cuboid geometry considered is on the scale of typical large rooms.

The first set of experiments (Bao et al., 2016), was performed in a concrete enclosure with a vent covered using glass of various strengths. To validate the model presented here, six different venting pressures, in the range 0.003 bar–0.55 bar, at a volumetric methane concentration of 6.5%, 9.5% and 12.5% ($\phi = 0.66, 1$ and 1.36), were simulated, with the test conditions listed in Table 2. Figs. 2–5 show the comparison between experiments [12] and the present simulation results of the EVA for the overpressure transients. Both experiments and simulations show that the magnitude of the overpressure spike increases with the vent pressure. In the EVA, the same time histories are experienced at different vent pressures, whereas, in the experiments, the time histories of different vent pressure cases are slightly shifted, mainly, because of the effect of the glass strength on the overpressure, which increases in the case of faster methane-air flames (Fig. 5). Therefore, the deviation between the experiment and the EVA simulations increases for faster methane-air flames. In the slowest burning case, of 12.5% volumetric concentration of the methane-air mixture, the lowest deviation between the experiments and the EVA simulation in overpressure transients is observed.

The EVA agrees reasonably well with the experimental data, both qualitatively and quantitatively. Some error exists because of the challenge in predicting the point of glass breakage. This is clearly observed in the experiment with an anticipated venting pressure of 0.54 bar, performed with a 12 mm float glass. The glass

breakage and consequent venting begins well before the predicted pressure, at approximately 0.33 bar.

It is noted that accounting for the effect of glass strength on the venting process requires considering of the interaction of fluids with solids, which is actually a complicated multi-physics process. For this reason, the effect of broken glass on the pressure is not implemented in the current version of the EVA, which, instead, simply considers an unvented enclosure until the enclosure pressure reaches the venting pressure listed in test cases of Bao et al. (2016). Incorporation of the effect of glass breaking into the EVA requires a separate work that will be undertaken elsewhere. In this respect, Fig. 3 compares the EVA and the experimental results for the venting pressure of 0.33 bar which actually corresponds on the glass broken case of 0.54. Good agreement between the simulation and experimental plots of Fig. 3 can justify that accounting for the effect of broken glass is not of crucial importance for the present simulations.

The second set of comparisons are based on the four experiments of Bauwens et al. (2008), which were conducted for an

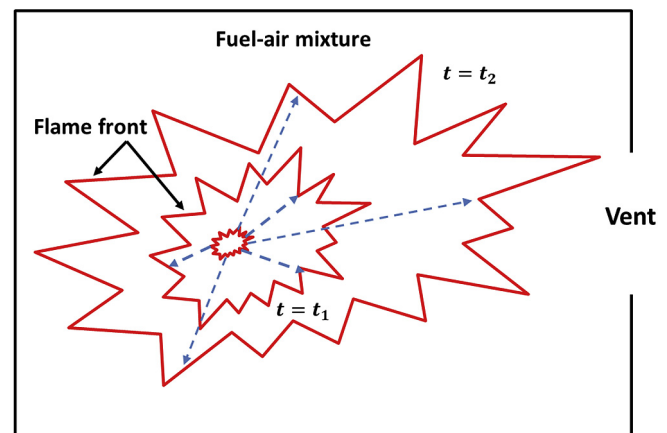


Fig. 1. Schematic representation of gas explosion in vented enclosures.

Table 1

The chronological development progress and limitations of EVA.

Mulpuru and Wilkin (1982)
Over pressure spikes for cylinders and spheres geometries zero-dimensional model derived from mass and energy balances Rear and central ignition was considered for vented enclosures The model consider only hydrogen air mixtures
Ugarte et al. (2016)
Enclosure shapes: Cylinder, Cuboid, Sphere Rear and central ignition was considered for vented enclosures Flame shape was estimated based on experimental images from Cooper et al. (1986)
Present work
Flame speed equations for methane and propane based on the experimental study of Stone et al. (1998), Liao et al. (2004) Integration of EVA with NASA-CAE code to calculate the thermo physical properties of any combustible gas mixture Validation with methane-air mixture experiments parametric analysis based on vent size and equivalent ratio

initially-open vent in a cuboid enclosure and supported by a CFD model to calculate the pressure in the same geometries. The simulations were performed with a solver based on the OpenFOAM, an open source CFD toolbox. The OpenFOAM can solve the mass, momentum, energy, and species transport equations for laminar and turbulent flows. The turbulent flow is solved by means of the large eddy simulations (LES) in the OpenFOAM. The geometry consisted of 10^6 cells and requires the inclusion of a $10 \times 6 \times 7.6$ m external volume. Herein, the present model is used to simulate the geometries of Bauwens et al. (2008), as shown below in Figs. 6–9.

In the first simulation, Fig. 6, while the timing of the first pressure spike is estimated accurately the quantity of the pressure spike. The pressure spike in the experimental data is seen to be greater than that of the EVA or the CFD simulations. As shown in Fig. 6, the magnitude of the spike predicted by EVA is slightly more accurate than the CFD model, however also predicts a larger pressure drop after the initial spike, compared with the experiment. Once the flame reaches the vent area, the flame area is significantly reduced, hence the burning and the internal pressure decreases significantly. This event is responsible for the large pressure drop after the first pressure spike.

The second simulation, Fig. 7, shows the largest discrepancy between the EVA and the experimental data. Namely, while the EVA predicts the time of the pressure spike accurately, it overestimates the magnitude of the spike by almost three times. This discrepancy is because of flame-acoustic interactions, which are accounted by the CFD model, but not included in the current version of the EVA. Fig. 7 also shows a second pressure spike in the experimental data, which is predicted by the CFD model. This spike is caused by the unburned gas in the enclosure that burns, rapidly after the flame has reached the vent. This spike is observed in the case of rear ignition, but not for central ignition, because when the flame is ignited in the rear, it travels through the entire enclosure to reach the vent, consuming on this way most of the fuel. Central ignition, however, can leave a large amount of unburned gas in the rear of the enclosure. Due to the acoustic effects and large surface area of the flame, this remaining gas may be burnt, rapidly, thereby creating a large, second pressure spike, which may appear larger than the first spike.

The third simulation, Fig. 8, is also for rear ignition, but with a larger vent size. As expected for rear ignition, there is no second large pressure spike here. While both the CFD model and the EVA underestimate the pressure spike, the latter is again more accurate than the CFD prediction. The large pressure spike, followed by the immediate drop, can presumably be devoted to the effects of the external explosion preventing venting, and its coupling to the acoustic.

The fourth simulation is shown in Fig. 9. In this case, it is seen that the EVA is significantly more accurate at predicting the initial pressure spike than the CFD model. While the second pressure

Table 2

Venting pressure and the vent cover considered in EVA simulations and experiments by Bao et al.

Volumetric concentration of methane = 6.5%, 9.5% and 12.5% ($\phi = 0.66, 1, \text{ and } 1.36$)	
Vent cover	Venting pressure (bar)
Polyethylene film	0.003
4 mm float glass	0.073
5 mm float glass	0.101
8 mm float glass	0.21
12 mm float glass	0.54
5 mm tempered glass	0.55

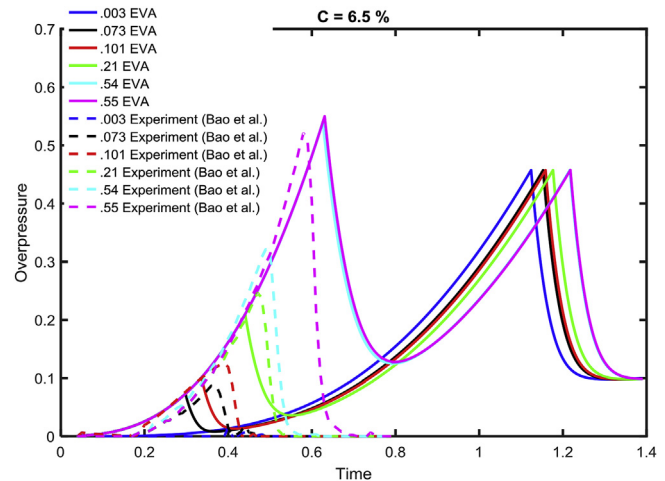


Fig. 2. Overpressure vs time for various venting pressures. EVA solution and experimental data for 6.5% of methane-air mixture (Bao et al., 2016).

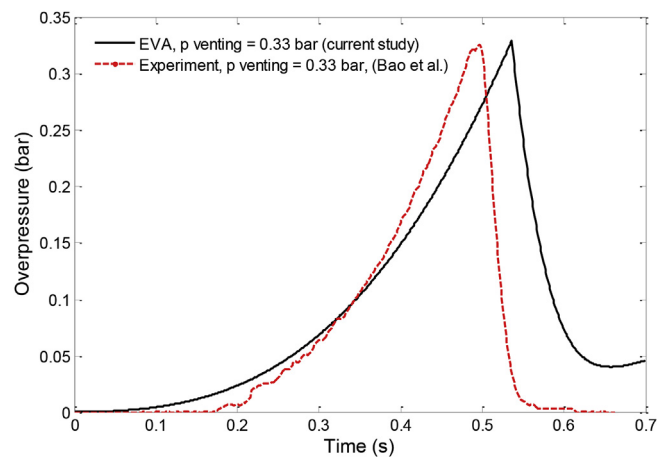


Fig. 3. Overpressure vs time for broken glass case of venting pressure of 0.54 bar. (The vent cover was broken when venting pressure reached 0.33 bar). A comparison of the EVA solution and experimental data (Bao et al., 2016).

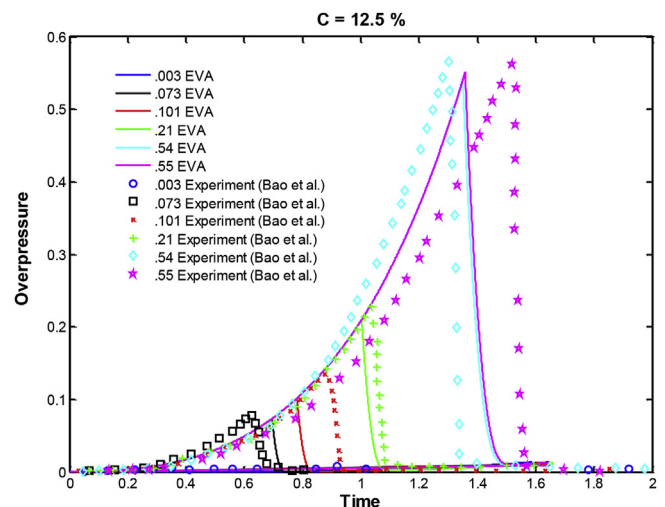


Fig. 4. Overpressure vs time for various venting pressures. EVA solution and experimental data for 12.5% of methane-air mixture (Bao et al., 2016).

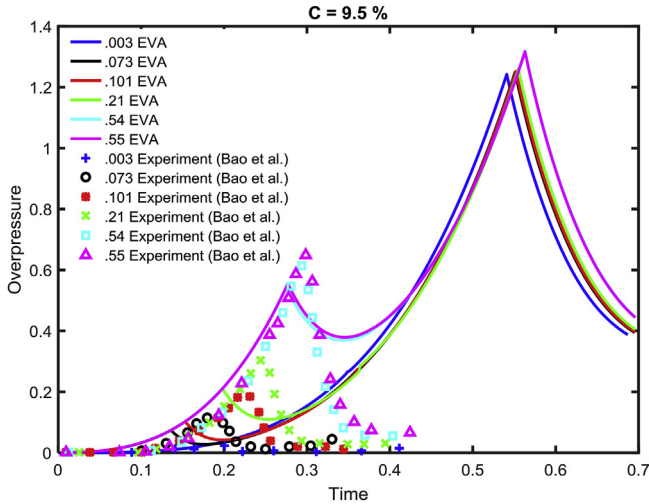


Fig. 5. Overpressure vs time for various venting pressures. EVA solution and experimental data for 9.5% of methane-air mixture (Bao et al., 2016).

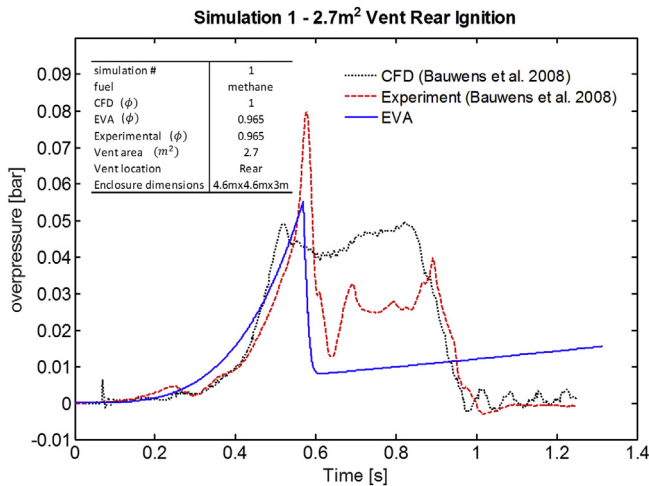


Fig. 6. Overpressure versus time for near stoichiometric methane-air mixtures a 2.7 m² vent and rear ignition.

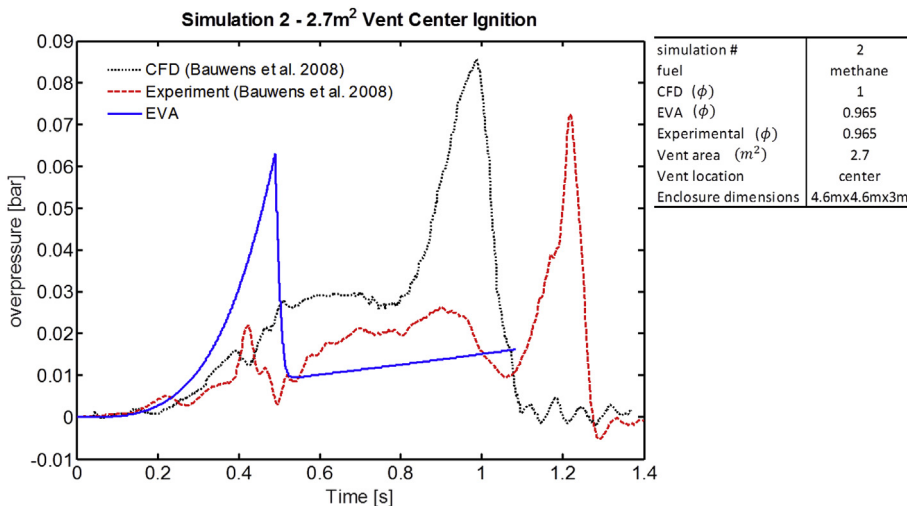


Fig. 7. Overpressure versus time for near stoichiometric methane-air mixtures a 2.7 m² vent and center ignition.

spike is not calculated here, the maximum overpressure, which is the main concern in safety, is predicted more accurately with the EVA than with the CFD model.

It is recalled that these four EVA simulations, Figs. 6–9, validated by the experiments (Bauwens et al., 2008), were conducted to verify EVA's accuracy as compared to a full CFD model. In this light, we can conclude that the EVA is successfully validated for the rear ignition geometries. However, this is not the case for central ignition, when the physics is more complex, in particular, because of a fresh fuel mixture remaining in the enclosure when the flame reaches the vent. Nevertheless, despite the errors in predicting the second spike for central ignition, the magnitude of the maximum pressure is consistently predicted well, as shown in Table 3, which compares the accuracies of the EVA and the CFD model to predict the maximum overall pressure spike.

The third set of the comparison are based on the peak pressure predicted by the NFPA 68, the EVA simulations, and the experimental data reported in Bao et al. (2016) and Bauwens et al. (2008). NFPA calculations are performed for 6.5%, 9.5 and 12.5% volumetric methane concentrations in a cuboid of 2m × 2m × 3m with a 0.64 m² of vent area. In NFPA 68 standards the thermo-physical parameters are given for fuel volumetric concentration below 5%. However, experiments and CFD calculations reported in Bao et al. (2016), Bauwens et al. (2008) were performed the volumetric methane concentrations in the range from 6.5% to 12.5%. Therefore, in this study, the thermos-physical parameters, the specific heats ratio for burnt gas-air mixture, Y_b , unburnt gas-air mixture dynamic viscosity μ , sound speed a_u , and mass density ρ_u are determined by the NASA CAE chemical equilibrium code. Parameters used in NFPA 68 calculations for stoichiometric methane-air mixture are listed in Table 5. Table 6 presents the maximum overpressure predicted by NFPA 68, EVA and Bao et al. (2016). The magnitude of the maximum overpressure predicted by NFPA 68 is 2–3 times larger than the experimental data by Bao et al. (2016) and EVA predictions. In Table 3, NFPA 68 calculations are performed for larger vent area at stoichiometric methane-air mixture. The NFPA predictions are larger than the EVA predictions and data reported in Bauwens et al. about one order of magnitude. In industry, the NFPA 68 standards are used to predict the vent area to design a suitable vent and maximum over pressure for a designed vent. Therefore, NFPA 68 predictions are larger than that of experimental data to ensure safety in any extreme case.

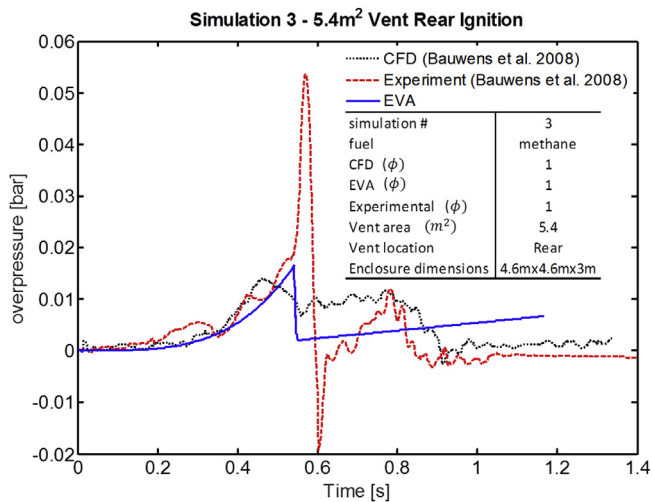


Fig. 8. Overpressure versus time for near stoichiometric methane-air mixtures a 5.4 m² vent and rear ignition.

5. Results and discussions

EVA simulations were performed to investigate the influence of the volumetric methane concentration in a vented cuboid enclosure of $4.5 \times 4.5 \times 3$ m, with the vent-to-wall area ratio 0.4, and the aspect ratio 1.53. Here, central spherical ignition was considered with the standard initial room temperature and pressure being 298 K and 1 atm, respectively. The volumetric concentrations of the fuel mixture, C, and the equivalent ratios, ϕ , employed in the simulations, are listed in Table 4.

Fig. 10 presents the evolution of the flame velocity (10a), vented mass (10b) and overpressure (10c) during the explosion time for the lean ($\phi = 0.8$), stoichiometric ($\phi = 1$) and rich ($\phi = 1.2$) methane-air mixtures in the vented cuboid enclosure. As observed in Fig. 10a, the deviation in the flame velocity is minor, with the maximal flame velocity values obtained at the stoichiometric methane-air conditions. The vented mass trends in Fig. 10c are similar for different equivalent ratios. However, again, the most ventilation of the mass occurs at stoichiometric conditions which certifies that the vented mass is significantly affected by the laminar flame speed. The evaluation of the internal overpressure is

Table 3

Error of maximum pressure prediction for EVA and CFD

Simulation #	1	2	3	4
Vent Size (m ²)	2.7	2.7	5.4	5.4
Vent Location	Rear	Center	Rear	Center
NFPA 68	3.485		0.3865	
EVA max pressure (bar)	0.0565	0.0631	0.0183	0.0204
CFD max pressure (bar)	0.0494	0.0858	0.0140	0.0174
Experimental max pressure (bar)	0.0796	0.0723	0.0536	0.0256
EVA error	29.0%	12.7%	65.9%	20.2%
CFD Error	37.9%	18.6%	73.9%	32.1%
NFPA Error	4278%		385%	

shown in Fig. 10b. Here, the internal pressure trends show two peaks in each case, which agrees with the computational observation by Ugarte et al. (2016) for a hydrogen-air mixture in a vented cuboid enclosure. The first internal pressure drop, observed in Fig. 10b, occurs when the flame reaches the vent area. The second drop is devoted to the external explosion. The detailed mechanism and formulation of the external explosion is given in Ref. (Ugarte et al., 2016)

A parametric study for various vent sizes, was also conducted by using EVA and NFPA 68, for both rear and center ignition of a stoichiometric fuel mixture, and the result is shown in Fig. 11.

Similar to the experiments (Bauwens et al., 2008), a cuboid enclosure of volume 60.7 m³ was considered, with the vent size to be in the range 0–12m². Maximum overpressure predicted by NFPA 68 is one order of magnitude higher than that of experiments and EVA simulations for this cuboid geometry. Here it should be noted that, the NFPA 68 results in higher over pressure predictions due to safety requirements. Fig. 11 shows that the initial decrease in maximum pressure is very rapid as venting area grows. For this geometry, a venting area of approximately 2 m² would be the minimum required to ensure an overpressure below 0.1 atm, which

Table 4

Equivalent ratios and volumetric concentration of fuel used in the simulations

Methane	
Φ	C [dimension]
0.8	0.0775
1	0.0951
1.2	0.1119

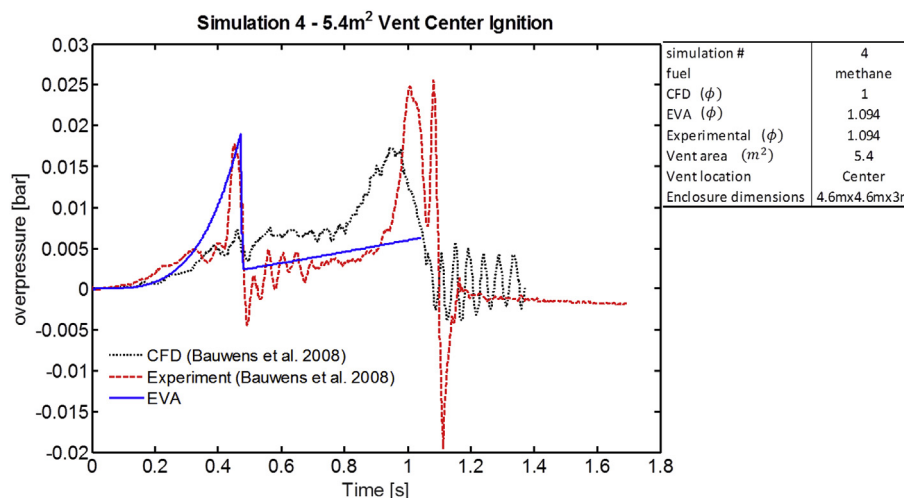


Fig. 9. Overpressure versus time for near stoichiometric methane-air mixtures a 5.4 m² vent and center ignition.

Table 5
Parameters used in NFPA calculations for stoichiometric methane-air mixture

Initial pressure, P_0 (bar-g)	0
Fundamental burning velocity, S_u (m/s)	0.37
The maximum pressure developed in a contained deflagration by ignition of the same gas-air mixture, P_{max}	7.1
Unburnt gas-air mixture dynamic viscosity μ , (kg/m-s)	1.8E-05
Unburnt gas-air mixture sound speed a_u , (m/s)	353
Unburnt gas-air mixture mass density ρ_u , (kg/m ³)	1.35
Ratio of specific heats for burned gas-air mixture γ_b	1.19
Unburnt gas-air mixture sonic flow mass flux, G_u , (kg/m ² -s)	230.1

Table 6
Maximum overpressure reported in Bao et al. (2016) and calculated with EVA and NFPA 68

Pstat	6.50%			9.50%			12.5		
	EVA	NFPA	Bao et al. (2016)	EVA	NFPA	Bao et al. (2016)	EVA	NFPA	Bao et al. (2016)
0.03	0.4574	0.9383	0.006	1.2422	1.2611	1.102	0.03	1.268	0.0039
0.073	0.4574	1.0054	0.095	1.249	1.3247	1.338	0.073	1.3328	0.079
0.101	0.4574	1.032	0.135	1.2519	1.349	1.22	0.101	1.3583	0.134
0.21	0.4574	1.1361	0.51	1.2592	1.4462	0.82	0.21	1.4578	0.229
0.54	0.5402	1.4428	0.54	1.3179	1.7367	0.646	0.54	1.7529	0.564
0.55	0.55	1.452	0.7	1.3167	1.7459	0.95	0.55	1.7621	0.568

is the point at which fatal injuries occur. Also, the maximum overpressure asymptotically approaches zero for the large venting areas.

6. Conclusions

In this paper, an in-house phenomenological computational model for gas explosions venting (the Explosion Venting Analyzer; EVA), which was recently developed and validated on hydrogen

explosions by Ugarte et al. (2016), is further extended to methane explosions. It is demonstrated that EVA can predict the initial pressure spikes with accuracy similar to that of full CFD models. Indeed, out of four EVA simulations validated by the experiments (Bauwens et al., 2008), Figs. 6–9, the two with rear ignition demonstrated more accurate predictions than the CFD. As for center ignition, while the second pressure spike is not predicted, the overall maximum pressure is nevertheless predicted accurately by the EVA. These results are considered to be good enough keeping

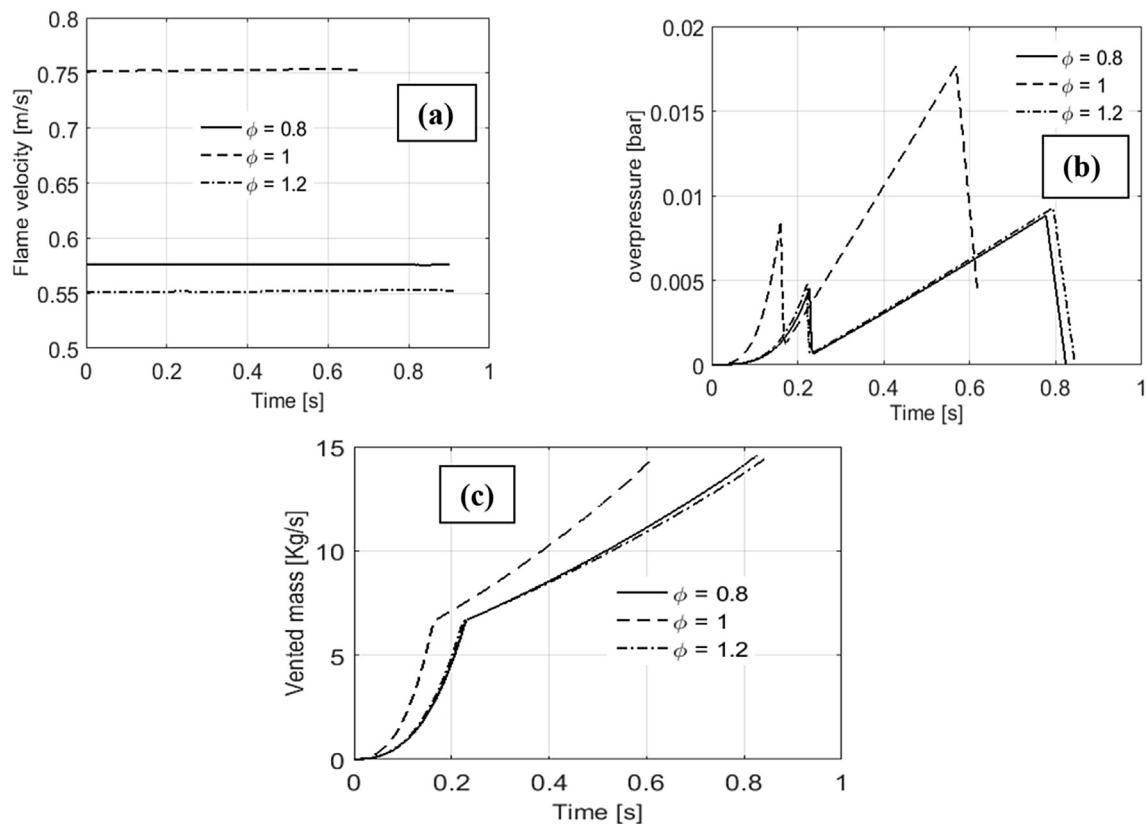


Fig. 10. a) Flame velocity b) Vented mass c) Overpressure transients at $\phi = 0.8, 1, 1.2$ for methane-air mixture in a cuboid.

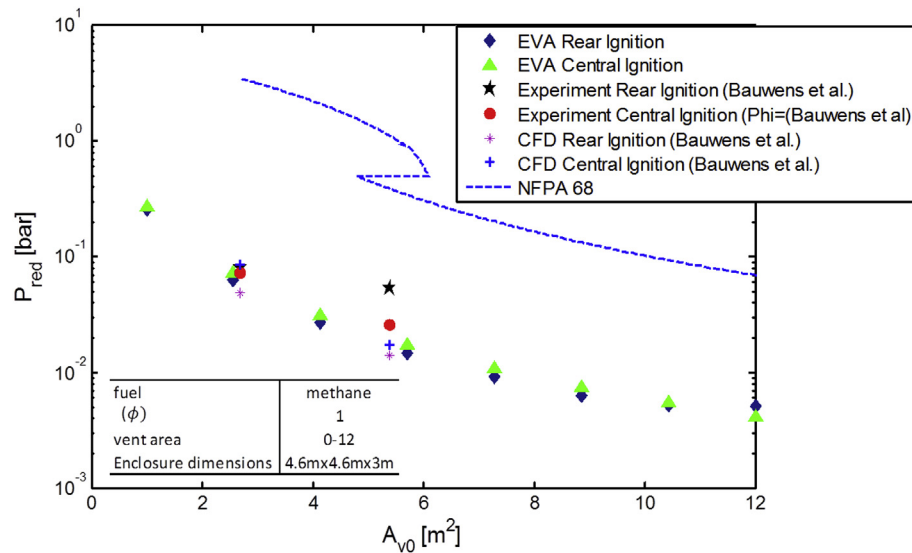


Fig. 11. Parametric study of maximum overpressure where the area is varied in the range 0–12m².

in mind a significant reduction in computing powered to run the EVA as compared to a standard (3-D) CFD software.

This reduction in required computing power yields several advantages. First, and foremost, this allows the computational data to be obtained promptly. Second, the risk of losing time by running simulations with potentially incorrect inputs is reduced. Finally, it allows parametric studies (such as that for various vent sizes; Fig. 11) to be completed promptly. EVA is also compared to the NFPA 68 standards which is used in industry widely for vent design and maximum overpressure predictions. The NFPA predictions are one order of magnitude higher than that of experiments and EVA predictions when large vent area and enclosure volume is used (see Fig. 11). However, the difference between NFPA and EVA decreases when small enclosure volume and vent area is used.

With the potential usage of EVA in fire safety and building design, the model should be easy to learn, employ and modify. More importantly, however, this means that the model must be accurate for all geometries. While the version presented here predicts the maximum overpressure well, as compared to the CFD model, the second pressure spike witnessed in central ignition geometries is not seen. To do this, some modifications can be undertaken in the future. In particular, approximating the increased burning rate and flame shape in late stages can improve the accuracy.

Acknowledgements

We thank Jerome Taveau of FIKE Corporation and Arvind Thiruvengadam of West Virginia University for useful discussions. This work is supported by the US National Science Foundation (NSF) through CAREER Award #1554254 (V.A.).

References

Bao, Qi, Fang, Q., Zhang, Y., Chen, L., Yang, S., Zhan, L., 2016. Effects of gas

- concentration and venting pressure on overpressure. *Fuel* 175, 40–48.
- Bauwens, C.R., Chaffee, J., Dorofeev, S.B., 2011. Vented explosion overpressures from combustion of hydrogen and hydrocarbon mixtures. *Int. J. hydrogen energy* 36 (3), 2329–2336.
- Bauwens, C.R., Chaffee, J., Dorofeev, S., 2008. Experimental and Numerical Study of Methane-air Deflagrations in a Vented Enclosure. s.l., s.n, pp. 1043–1054.
- Cooper, M.G., Fairweather, M., Tite, J.P., 1986. On the mechanisms of pressure generation in vented explosions. *Combust. Flame* 65 (1), 1–14.
- Faghii, M., Gou, X., Chen, Z., 2016. The explosion characteristics of methane, hydrogen and their mixtures: a computational study. *J. Loss Prev. Process Industries* 131–138.
- Forcier, T., Zalosh, R., 2000. External pressures generated by vented gas and dust explosions. *J. Loss Prev. Process Industries* 13 (3), 411–417.
- Sanford, Gordon, McBride, Bonnie J., 1996. Computer Program for Calculation of Complex Chemical Equilibrium Compositions and Applications, s.l. National Aeronautics and Space Administration, Office of Management, Scientific and Technical Information Program.
- Harrison, A.J., Eyre, J.A., 1987. External explosions as a result of explosion venting. *Combust. Sci. Technol.* 52 (1–3), 91–106.
- Liao, S.Y., Jiang, D.M., Cheng, Q., 2004. Determination of laminar burning velocities for natural gas. *Fuel* 83, 1247–1250.
- Molkov, V., Dobashi, R., Suzuki, M., Hirano, T., 2000. Venting of deflagrations: hydrocarbon–air and hydrogen–air systems. *J. Loss Prev. Process Industries* 13 (3), 397–409.
- Mulpuru, S.R., Wilkin, G.B., 1982. A Model for Vented Deflagration of Hydrogen in a Volume, s.l. Atomic Energy of Canada Ltd.
- NFPA 68, 2013. Standard on Explosion Protection by Deflagration Venting. s.l.: NFPA.
- Sezer, H., Akkerman, V., Ugarte, O.J., Rangwala, A.S., 2016. Methane- and Propane-induced Explosions in Vented Enclosures. Princeton, s.n.
- Sharma, S.P., Agrawal, D.D., Gupta, C.P., 1981. The pressure and temperature dependence of burning velocity in a spherical combustion bomb. *Symposium Int. Combust.* 18 (1), 493–501.
- STANDARD, B., 2008. Dust Explosion Venting Protective Systems. s.l.: s.n.
- Stone, Richard, Clarke, Andrew, Beckwith, Paul, 1998. Correlations for the laminar-burning velocity of methane/diluent/air mixtures obtained in free-fall experiments. *Combust. Flame* 114 (3), 546–555.
- Tamanini, Francesco, Valiulis, John V., 1996. Improved guidelines for the sizing of vents in dust explosions. *J. Loss Prev. Process Industries* 9 (1), 105–118.
- Ugarte, Orlando J., Akkerman, V'yacheslav, Rangwala, Ali S., 2016. A computational platform for gas explosion venting. *Process Saf. Environ. Prot.* 99, 167–174.
- Zalosh, R., 2008. Explosion Venting Data and Modeling Research Project. The Fire Protection Research Foundation, Massachusetts, USA.